Supporting Information

Introduction of flexibility into a metal-organic framework to promote Hg(II) capture through adaptive deformation

Jiayue Tian,[†‡,§] Chengdan Shi,[†‡] Cao Xiao,[‡] Feilong Jiang,[‡] Daqiang Yuan,[‡] Qihui Chen,[‡] and Maochun Hong*[‡]*

‡ State Key Laboratory of Structure Chemistry, Fujian Institute of Research on the Structure of Matter, Chinese Academy of Sciences, Fuzhou 350002, P. R. China

§ College of Material and Chemical Engineering, Zhengzhou University of Light Industry, Zhengzhou 450001, P. R. China

* Corresponding authors: chenqh@fjirsm.ac.cn; hmc@fjirsm.ac.cn.

† These authors contributed equally to this work.

Single-crystal structure determination:

The single-crystal X-ray diffraction data of **FJI-H30** and **FJI-H30-Hg** were collected on a SuperNova diffractometer using Cu Kα radiation (λ = 1.54184 Å) at 100 K. The obtained data were processed with *OLEX-2* software.[1] The structure were solved with the *ShelXT* structure solution program using Intrinsic Phasing method and refined with the *ShelXL* refinement package using Least Squares minimisation technique.[2] The detailed crystallographic data and structural refinement parameters are presented in Table S1.

Supporting figures and tables

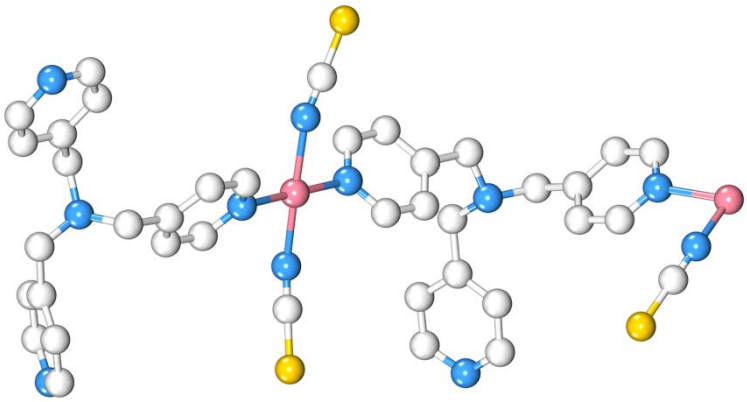

Figure S1. The asymmetric unit of **FJI-H30**.

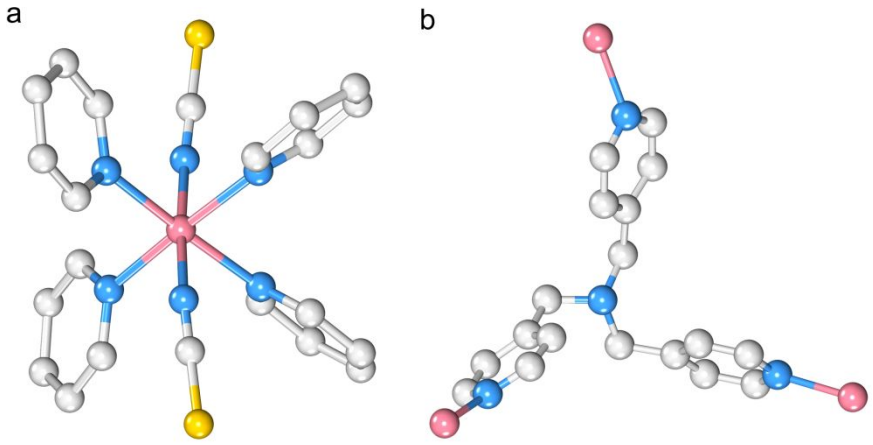

Figure S2. (a) The coordination environments of Co(II). (b) The linking mode of TPMA ligands in **FJI-H30**.

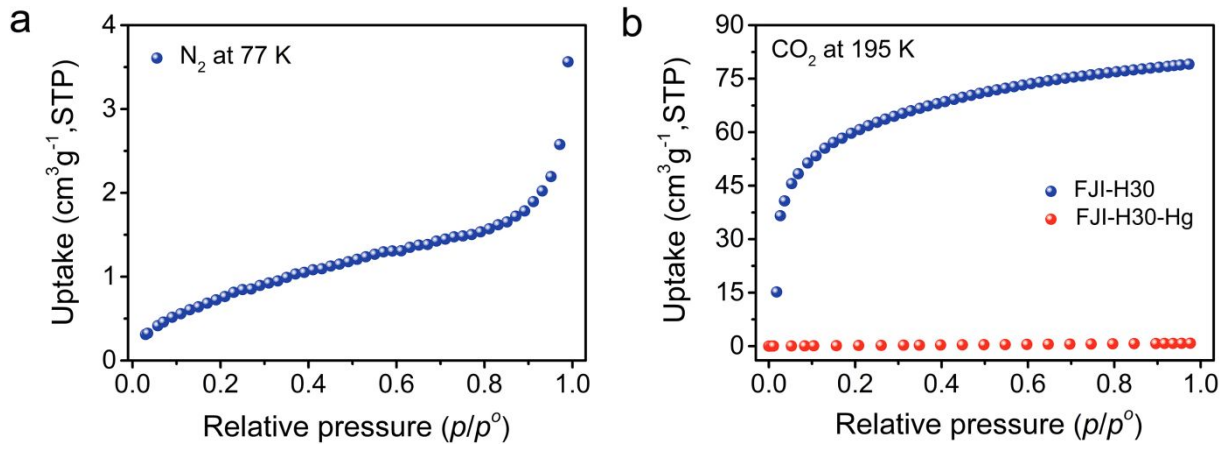

Figure S3 (a) N_2 adsorption isotherm of **FJI-H30** at 77 K. (b) CO_2 adsorption isotherms of **FJI-H30** and **FJI-H30-Hg** at 195 K.

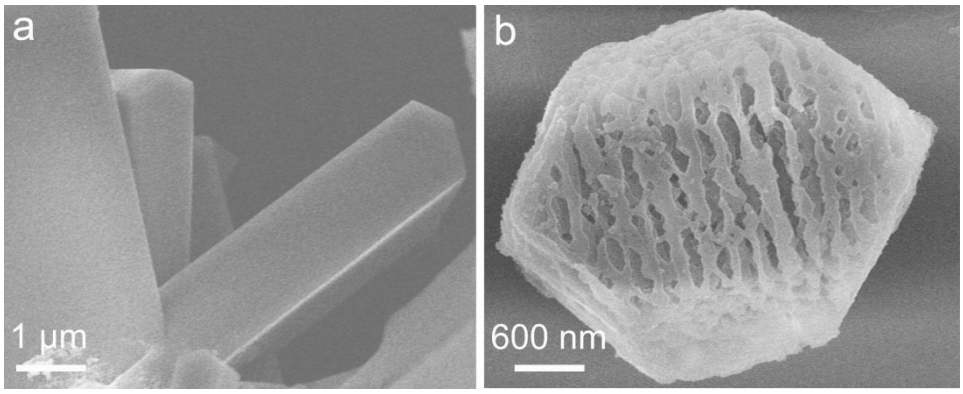

Figure S4. The SEM images of (a) **FJI-H30** and (b) **FJI-H30** treated after temperature-dependent PXRD tests from 30 to 150 ℃.

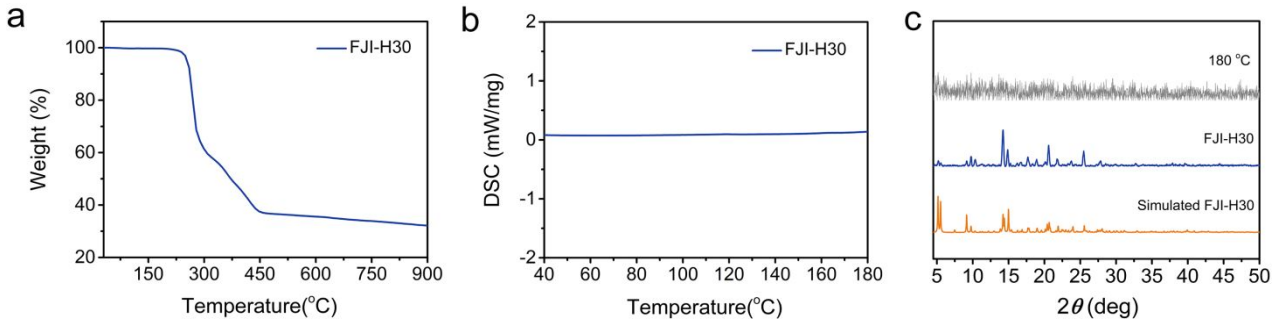

Figure S5. (a) The TG curve for **FJI-H30**. (b) DSC curve for **FJI-H30**. (c) The PXRD pattern of **FJI-H30** at 180 °C.

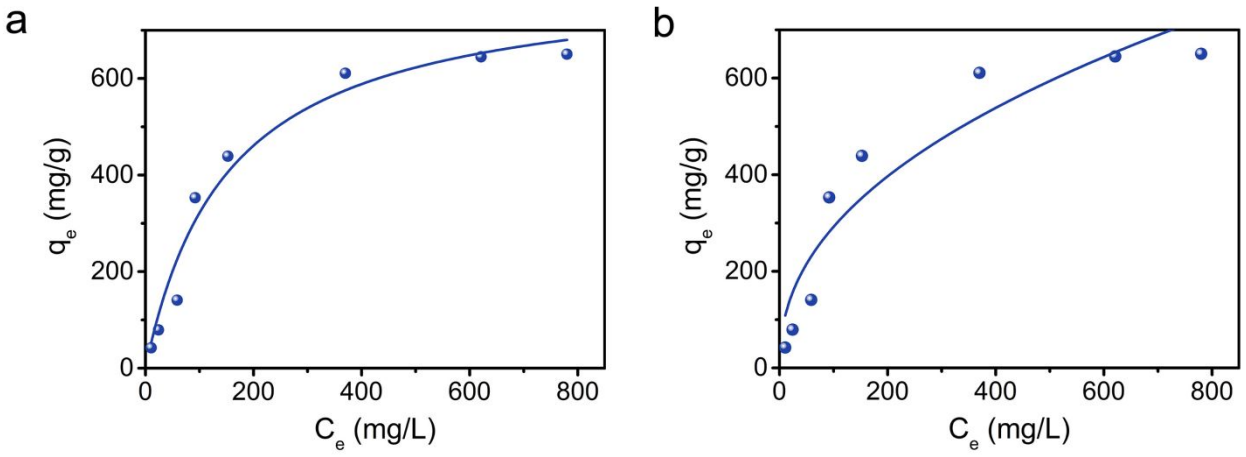

Figure S6. (a) The equilibrium adsorption data fitted by Langmuir adsorption model. (b) The equilibrium adsorption data fitted by Freundlich adsorption model.

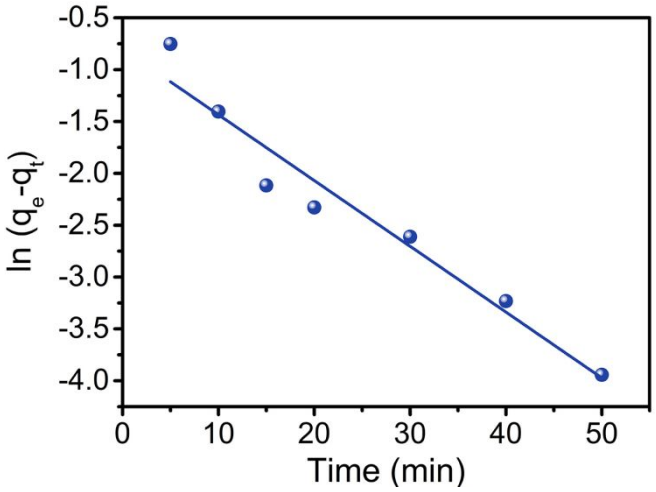

Figure S7. The pseudo-first-order kinetic plot for Hg(II) adsorption of **FJI-H30**.

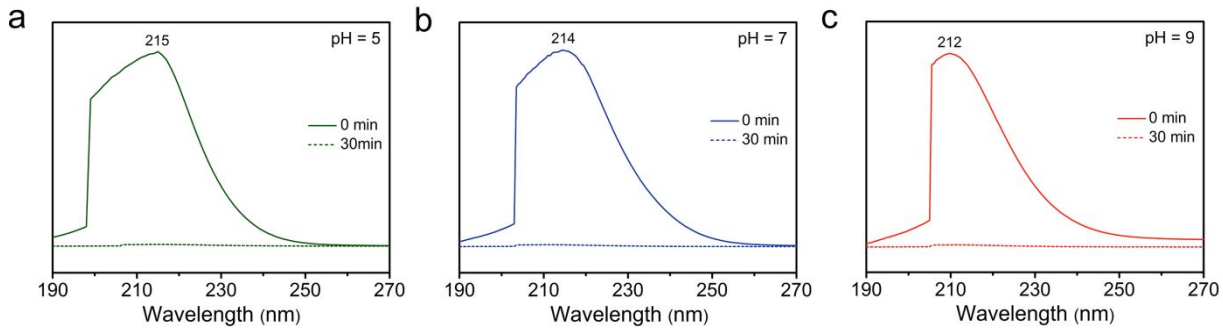

Figure S8. UV–Vis absorption spectra of the adsorption process of Hg(II) ions on **FJI-30** in $HgCl_2$ aqueous solution with pH = 5, 7 and 9.

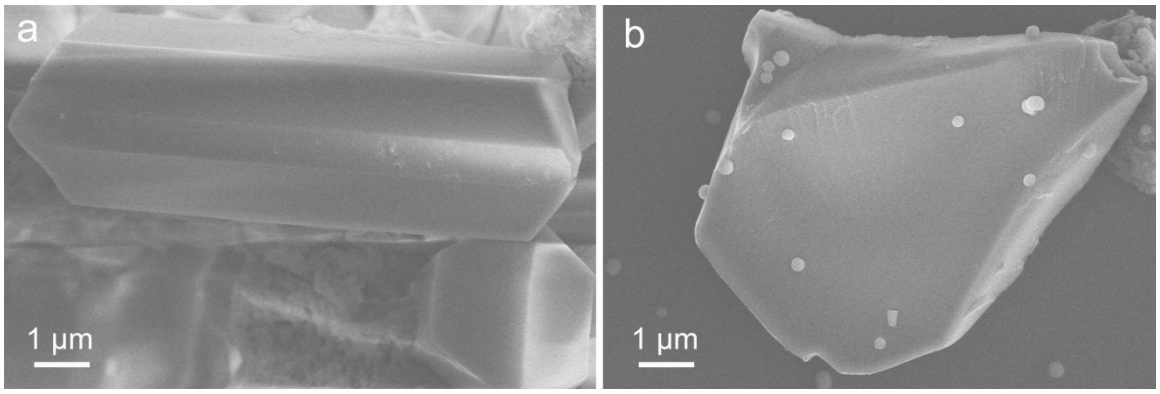

Figure S9. The SEM images of (a) **FJI-H30** and (b) **FJI-H30-Hg**.

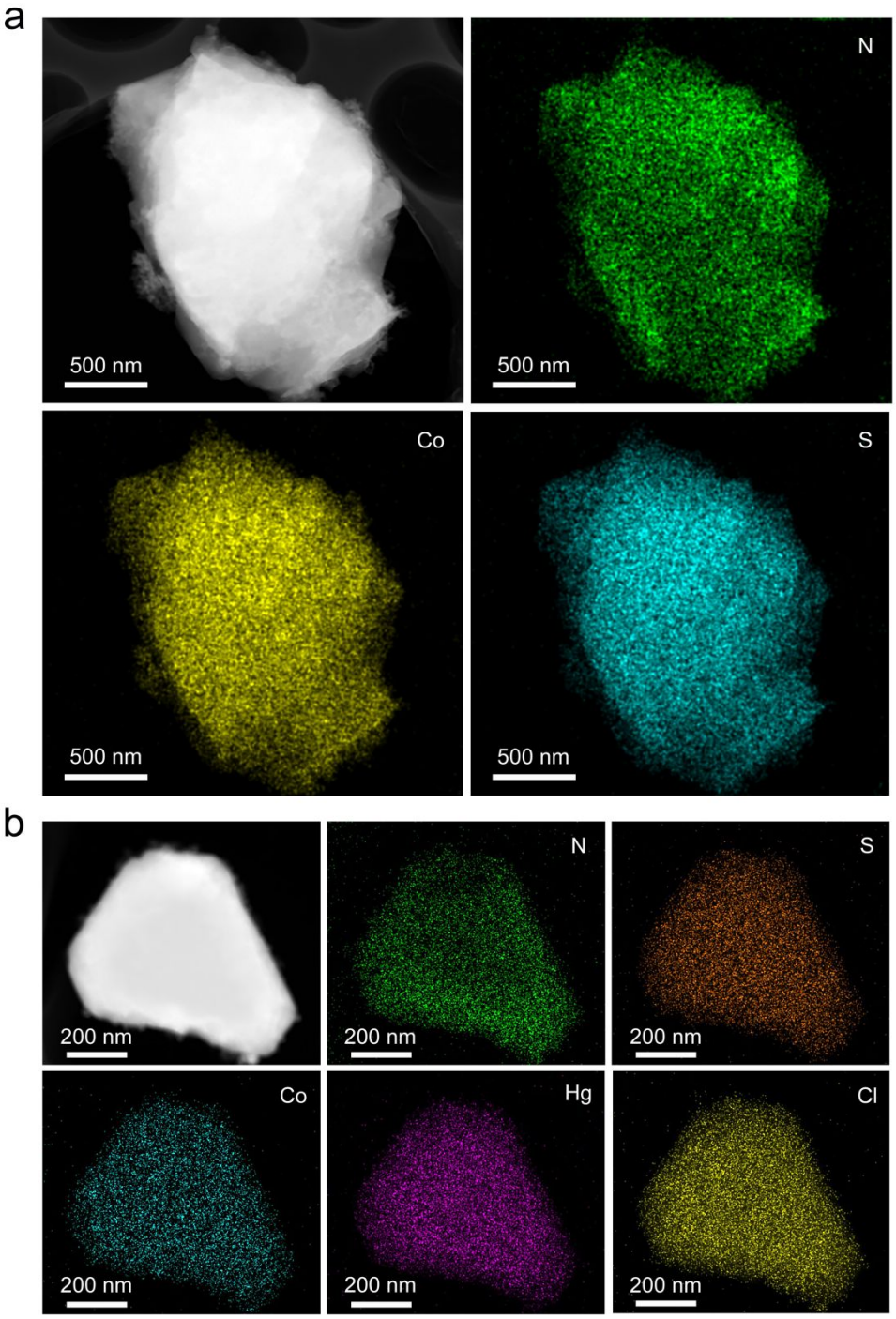

Figure S10. The HAADF-STEM images and corresponding elemental mapping of (a) **FJI-H30** and (b) **FJI-H30-Hg**.

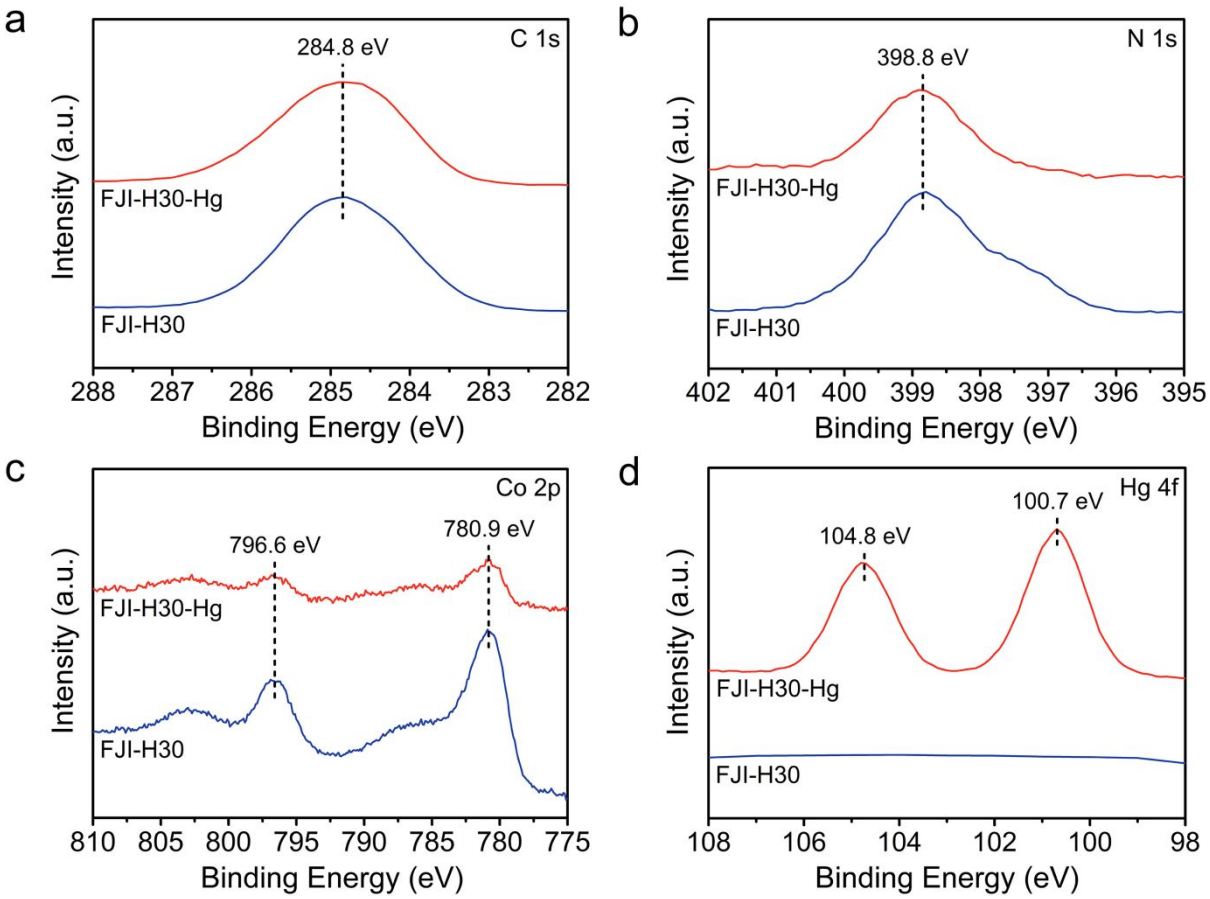

Figure S11. High-resolution XPS spectra for (a) C 1s, (b) N 1s, (c) Co 2p and (d) Hg 4f of **FJI-H30** and **FJI-H30-Hg**.

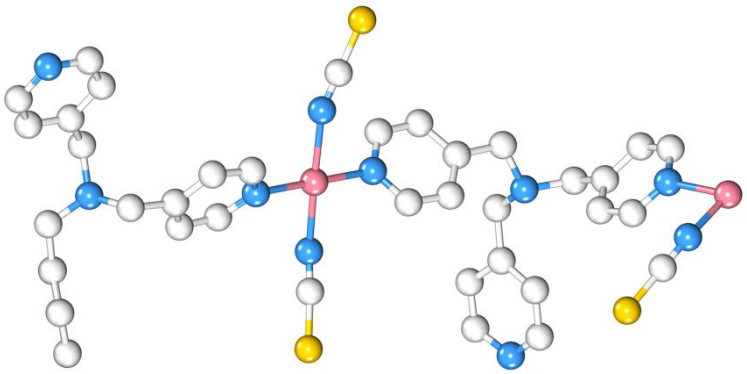

Figure S12. The asymmetric unit of **FJI-H30-Hg**.

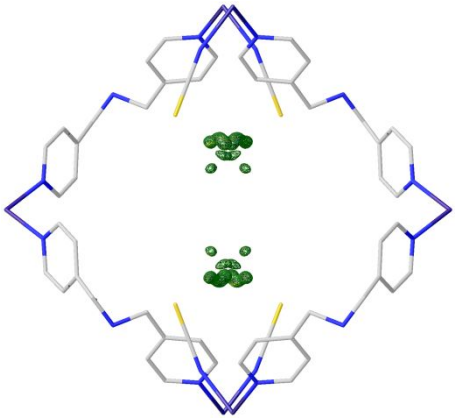

Figure S13. The electron density map of **FJI-H30-Hg**.

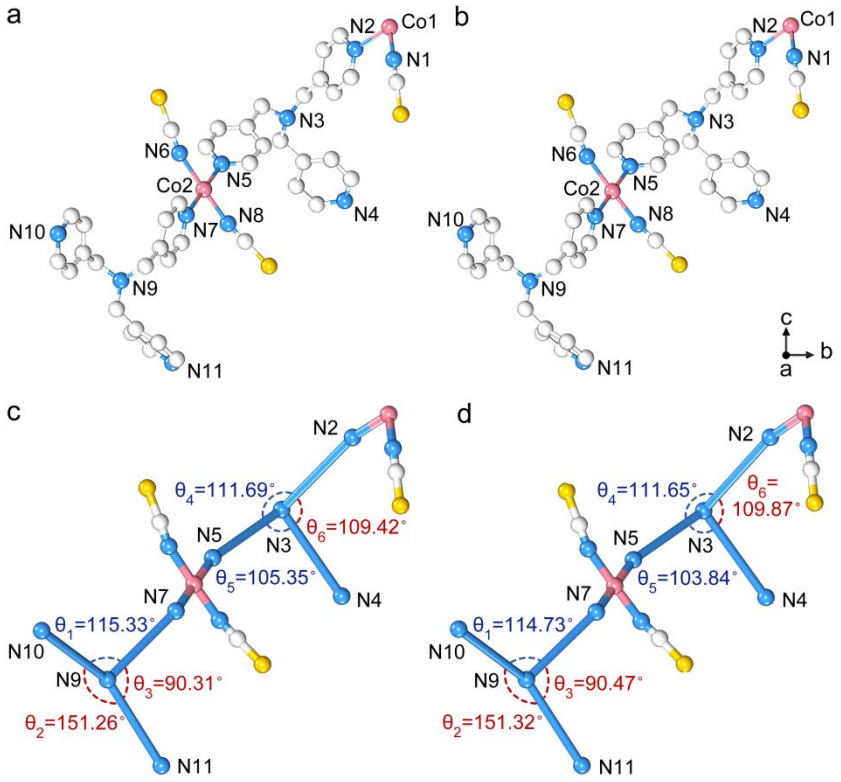

Figure S14. Contrast of the ligand conformation. The assymetric units of (a) **FJI-H30** and (b) **FJI-H30-Hg**. The angles of the abbreviated flexible linkage in (c) **FJI-H30** and (d) **FJI-H30-Hg**. The angles of the abbreviated ligands were measured by setting the tertiary amine nitrogen atoms as angular vertexes, and the linear connection between tertiary amine nitrogen atoms and pyridine nitrogen atoms as the two sides of these angles. Only the angles along *c* axis (θ_2, θ_3 and θ_6), marked with red, all enlarge from **FJI-H30** to **FJI-H30-Hg**, which corresponding to the expansion along *c* axis of pore A.

Table S1. Crystal data and structure refinement for **FJI-H30** and **FJI-H30-Hg**.

Compound reference	**FJI-H30**	**FJI-H30-Hg-framework**
Chemical formula	$C_{78}H_{72}Co_3N_{22}S_6$	$C_{78}H_{72}Co_3N_{22}S_6$
Formula weight	1686.72	1686.72
Temperature (K)	100.0(5)	100(1)
Crystal system	monoclinic	monoclinic
Space group	*I*2/*a*	*I*2/*a*
a / Å	15.7038(5)	15.6580(2)
b / Å	18.1035(8)	17.9736(2)
c / Å	34.5205(11)	34.6649(4)
α / °	90	90
β / °	96.857(3)	96.3780(10)
γ / °	90	90
Volume / Å^3	9743.8(6)	9695.4(2)
Z	4	4
D / g cm^{-3}	1.150	1.156
μ / mm^{-1}	5.537	3.773
F (000)	3484.0	3484.0
R_{int}	0.0674	0.0376
Goodness-of-fit on F^2	1.046	1.057
R_1 / ωR_2 [$I > 2\sigma(I)$]	0.0721 / 0.1987	0.0383 / 0.1046
R_1 / ωR_2 [all data]	0.0844 / 0.2132	0.0455 / 0.1084
CCDC number	2008378	2018724

Table S2. The contents of C, H, N elements in **FJI-H30** and **FJI-H30-Hg** obtained from the theoretical calculation of molecular formulas and experimental tests by elemental analysis.

Contents (%)	**FJI-H30**		**FJI-H30-Hg**	
	Cal.	Exp.	Cal.	Exp.
C	55.49	55.16	28.23	28.49
H	4.27	4.48	2.17	2.14
N	18.26	17.83	9.29	9.25

Table S3. Adsorption isotherm parameters for Hg(II) adsorption on **FJI-H30**.

Sample	$q_{m,\,exp}$	Langmuir adsorption isotherm			Freundlich adsorption isotherm		
		$q_{m,cal}$	K_L	R^2	K_F	n	R^2
FJI-H30	705	813	0.0066	0.9652	38.3928	0.4408	0.8873

Table S4. Kinetic parameters for Hg(II) adsorption on **FJI-H30**.

Sample	$q_{e,\,exp}$	Pseudo-first-order models			Pseudo-second-order models		
		k_1	$q_{e,\,cal}$	R^2	k_2	$q_{e,\,cal}$	R^2
FJI-H30	9.9395	0.5040	10.2677	0.9381	0.5040	9. 9582	>0.9999

Table S5. Summary of Hg(II) adsorption capacity in recently reported MOF absorbents.

Absorbents	Adsorption sites	Hg(II) adsorption capacity (mg g^{-1})	Ref
FJI-H30	thiocyanate	705	This work
FJI-H12	thiocyanate	439.8	3
TMU-40	free nitrogen	269	4
Zr-MSA	thiol	734	5
Bio-MOF	methionine	666	6
Cys-UiO-66	thiol	350.14	7
LMOF-263	sulfone	380	8
SH-MIL-68(In)	thiol	450	9
UiO-66DMTD	thiol	670.5	10
Zr-DMBD	thiol	171.5	11
Zr-DMBD	thiol	197	12
Zr-M1	thioether	275	13
Zr-L4	thioether	322	14
ZrOMTP	thiol	403	15
TMU-31	urea	476.19	16
CoCNSP	thiocyanate	716	17
NENU-401	thioether	600	18

Table S6. Contrast of the Hg(II) adsorption capacity for **FJI-H30** and recently reported COF absorbents.

Absorbents	Adsorption sites	Hg(II) adsorption capacity (mg g^{-1})	Ref
FJI-H30	thiocyanate	705	This work
COF-LZU8	thioether	236	19
COF-S-SH	thiol	588.2	20
TAPB-BMTTPA-COF	thioether	734	21
COF-S-SH	thiol	1350	22

References

1. Dolomanov, O. V.; Bourhis, L. J.; Gildea, R. J.; Howard, J. A. K.; Puschmann, H. OLEX2: A Complete Structure Solution, Refinement and Analysis Program. *J. Appl. Crystallogr.* **2009**, *42*, 339–341.

2. Sheldrick, G. M. SHELXT-Integrated Space-Group and Crystal-Structure Determination. *Acta. Cryst. A* **2015**, *71*, 3–8.

3. Liang, L.; Chen, Q.; Jiang, F.; Yuan, D.; Qian, J.; Lv, G.; Xue, H.; Liu, L.; Jiang, H.-L.; Hong, M. In situ Large-Scale Construction of Sulfur-Functionalized Metal-Organic Framework and Its Efficient Removal of Hg(II) from Water. *J. Mater. Chem. A* **2016**, *4*, 15370–15374.

4. Rouhani, F.; Morsali, A. Fast and Selective Heavy Metal Removal by a Novel Metal-Organic Framework Designed with In-Situ Ligand Building Block Fabrication Bearing Free Nitrogen. *Chem. Eur. J.* **2018**, *24*, 5529–5537.

5. Yang, P.; Shu, Y.; Zhuang, Q.; Li, Y.; Gu, J. A Robust MOF-based Trap with High-Density Active Alkyl Thiol for the Super-Efficient Capture of Mercury. *Chem. Commun.* **2019**, *55*, 12972–12975.

6. Mon, M.; Lloret, F.; Ferrando-Soria, J.; Martí-Gastaldo, C.; Armentano, D.; Pardo, E. Selective and Efficient Removal of Mercury from Aqueous Media with the Highly Flexible Arms of a BioMOF. *Angew. Chem. Int. Ed.* **2016**, *55*, 11167–11172.

7. Zhao, M.; Huang, Z.; Wang, S.; Zhang, L.; Zhou, Y. Design of L-Cysteine Functionalized UiO-66 MOFs for Selective Adsorption of Hg(II) in Aqueous Medium. *ACS Appl. Mater. Interfaces* **2019**, *11*, 46973–46983.

8. Rudd, N. D.; Wang, H.; Fuentes-Fernandez, E. M. A.; Teat, S. J.; Chen, F.; Hall, G.; Chabal, Y. J.; Li, J. Highly Efficient Luminescent Metal-Organic Framework for the Simultaneous Detection and Removal of Heavy Metals from Water. *ACS Appl. Mater. Interfaces* **2016**, *8*, 30294–30303.

9. Li, G.-P.; Zhang, K.; Zhang, P.-F.; Liu, W.-N.; Tong, W.-Q.; Hou, L.; Wang, Y.-Y. Thiol-Functionalized Pores via Post-Synthesis Modification in a Metal-Organic Framework with Selective Removal of Hg(II) in Water. *Inorg. Chem.* **2019**, *58*, 3409–3415.

10. Fu, L.; Wang, S.; Lin, G.; Zhang, L.; Liu, Q.; Fang, J.; Wei, C.; Liu, G. Post-Functionalization of UiO-66-NH_2 by 2,5-Dimercapto-1,3,4-thiadiazole for the High Efficient Removal of Hg(II) in Water. *J. Hazard. Mater.* **2019**, *368*, 42–51.

11. Ding, L.; Luo, X.; Shao, P.; Yang, J.; Sung, D. Thiol-Functionalized Zr-Based Metal-Organic Framework for Capture of Hg(II) through a Proton Exchange Reaction. *ACS Sustainable Chem. Eng.* **2018**, *6*, 8494–8502.

12. Yee, K.-K.; Reimer, N.; Liu, J.; Cheng, S.-Y.; Yiu, S.-M.; Weber, J.; Stock, N.; Xu, Z. Effective Mercury Sorption by Thiol-Laced Metal-Organic Frameworks: in Strong Acid and the Vapor Phase. *J. Am. Chem. Soc.* **2013**, *135*, 7795–7798.

13. Hou, Y.-L.; Yee, K.-K.; Wong, Y.-L.; Zha, M.; He, J.; Zeller, M.; Hunter, A. D.; Yang, K.; Xu, Z. Metalation Triggers Single Crystalline Order in a Porous Solid. *J. Am. Chem. Soc.* **2016**, *138*, 14852–14855.

14. He, Y.; Hou, Y.-L.; Wong, Y.-L.; Xiao, R.; Li, M.-Q.; Hao, Z.; Huang, J.; Wang, L.; Zeller, M.; He, J.; Xu, Z. Improving Stability Against Desolvation and Mercury Removal Performance of Zr(IV)-Carboxylate Frameworks by Using Bulky Sulfur Functions. *J. Mater. Chem. A* **2018**, *6*, 1648–1654.

15. Li, M.-Q.; Wong, Y.-L.; Lum, T.-S.; Sze-Yin Leung, K.; Lam, P. K. S.; Xu, Z. Dense Thiol Arrays for Metal-Organic Frameworks: Boiling Water Stability, Hg Removal Beyond 2 ppb and Facile Crosslinking. *J. Mater. Chem. A* **2018**, *6*, 14566–14570.

16. Hakimifar, A.; Morsali, A. Urea-Based Metal-Organic Frameworks as High and Fast Adsorbent for Hg^{2+} and Pb^{2+} Removal from Water. *Inorg. Chem.* **2019**, *58*, 180–187.

17. Li, J.; Duan, Q.; Wu, Z.; Li, X.; Chen, K.; Song, G.; Alsaedi, A.; Hayat, T.; Chen, C. Few-Layered Metal-Organic Framework Nanosheets as a Highly Selective and Efficient Scavenger for Heavy Metal Pollution Treatment. *Chem. Eng. J.* **2020**, *383*, 123189.

18. Jiang, S. Y.; He, W. W.; Li, S. L.; Su, Z. M.; Lan, Y. Q. Introduction of Molecular Building Blocks to Improve the Stability of Metal-Organic Frameworks for Efficient Mercury Removal. *Inorg. Chem.* **2018**, *57*, 6118–6123.

19. Ding, S.-Y.; Dong, M.; Wang, Y.-W.; Chen, Y.-T.; Wang, H.-Z.; Su, C.-Y.; Wang, W. Thioether-Based Fluorescent Covalent Organic Framework for Selective Detection and Facile Removal of Mercury(II). *J. Am. Chem. Soc.* **2016**, *138*, 3031–3037.

20. Li, Y.; Hu, T.; Chen, R.; Xiang, R.; Wang, Q.; Zeng, Y.; He, C. Novel Thiol-functionalized Covalent Organic Framework as Adsorbent for Simultaneous Removal of BTEX and Mercury (II) from Water. *Chem. Eng. J.* **2020**, *398*, 125566.

21. Huang, N.; Zhai, L.; Xu, H.; Jiang, D. Stable Covalent Organic Frameworks for Exceptional Mercury Removal from Aqueous Solutions. *J. Am. Chem. Soc.* **2017**, *139*, 2428–2434.

22. Sun, Q.; Aguila, B.; Perman, J.; Earl, L. D.; Abney, C. W.; Cheng, Y.; Wei, H.; Nguyen, N.; Wojtas, L.; Ma, S. Postsynthetically Modified Covalent Organic Frameworks for Efficient and Effective Mercury Removal. *J. Am. Chem.*

Soc. **2017**, *139*, 2786–2793.